6-2017

Retrieving landscape freeze/thaw state fromSoil Moisture Active Passive (SMAP) radar and radiometer measurements

C. Derksen

Xiaolan Xu

R. Scott Dunbar

Andreas Colliander

Youngwook Kim

See next page for additional authors

Recommended Citation

Chris Derksen, Xiaolan Xu, R. Scott Dunbar, Andreas Colliander, Youngwook Kim, John S. Kimball, T. Andrew Black, Eugenie Euskirchen, Alexandre Langlois, Michael M. Loranty, Philip Marsh, Kimmo Rautiainen, Alexandre Roy, Alain Royer, Jilmarie Stephens, Retrieving landscape freeze/thaw state from Soil Moisture Active Passive (SMAP) radar and radiometer measurements, Remote Sensing of Environment, Volume 194, 1 June 2017, Pages 48-62, http://doi.org/10.1016/j.rse.2017.03.007

Remote Sensing of Environment 194 (2017) 48–62

Contents lists available at ScienceDirect

Remote Sensing of Environment

journal homepage: www.elsevier.com/locate/rse

Retrieving landscape freeze/thaw state from Soil Moisture Active Passive (SMAP) radar and radiometer measurements

Chris Derksen [a,*], Xiaolan Xu [b], R. Scott Dunbar [b], Andreas Colliander [b], Youngwook Kim [c], John S. Kimball [c], T. Andrew Black [d], Eugenie Euskirchen [e], Alexandre Langlois [f], Michael M. Loranty [g], Philip Marsh [h], Kimmo Rautiainen [i], Alexandre Roy [f], Alain Royer [f], Jilmarie Stephens [d]

[a] Climate Research Division, Environment and Climate Change, Canada
[b] Jet Propulsion Laboratory, United States
[c] University of Montana, United States
[d] University of British Columbia, Canada
[e] University of Alaska-Fairbanks, United States
[f] Université de Sherbrooke, Canada
[g] Colgate University, United States
[h] Wilfrid Laurier University, Canada
[i] Finnish Meteorological Institute, Finland

ARTICLE INFO

Article history:
Received 13 October 2016
Received in revised form 8 February 2017
Accepted 9 March 2017
Available online xxxx

Keywords:
SMAP
Radar
Passive microwave
Freeze/thaw

ABSTRACT

Over one-third of the global land area undergoes a seasonal transition between predominantly frozen and non-frozen conditions each year, with the land surface freeze/thaw (FT) state a significant control on hydrological and biospheric processes over northern land areas and at high elevations. The NASA Soil Moisture Active Passive (SMAP) mission produced a daily landscape FT product at 3-km spatial resolution derived from ascending and descending orbits of SMAP high-resolution L-band (1.4 GHz) radar measurements. Following the failure of the SMAP radar in July 2015, coarser (36-km) footprint SMAP radiometer inputs were used to develop an alternative daily passive microwave freeze/thaw product. In this study, in situ observations are used to examine differences in the sensitivity of the 3-km radar versus the 36-km radiometer measurements to the landscape freeze/thaw state during the period of overlapping instrument operation. Assessment of the retrievals at high-latitude SMAP core validation sites showed excellent agreement with in situ flags, exceeding the 80% SMAP mission accuracy requirement. Similar performance was found for the radar and radiometer products using both air temperature and soil temperature derived FT reference flags. There was a tendency for SMAP thaw retrievals to lead the surface flags due to the influence of wet snow cover conditions on both the radar and radiometer signal. Comparison with other satellite derived FT products showed those derived from passive measurements (SMAP radiometer; Aquarius radiometer; Advanced Microwave Scanning Radiometer - 2) retrieved less frozen area than the active products (SMAP radar; Aquarius radar).

1. Introduction

Within the terrestrial cryosphere, spatial patterns and timing of landscape freeze/thaw (FT) state transitions are highly variable with measurable impacts to climate, hydrological, ecological and biogeochemical processes. Landscape FT state influences the seasonal amplitude and partitioning of surface energy exchange, while ecosystem responses to seasonal thaw are rapid, with evapotranspiration, soil respiration, and plant photosynthetic activity accelerating with warmer temperatures and the availability of liquid water (Panneer Selvam et al., 2016; Zhang et al., 2011; Chapin et al., 2005; Black et al., 2000; Jarvis and Linder, 2000). The annual non-frozen period also bounds the vegetation growing season, while variability in FT timing has a direct impact on vegetation net primary production and net ecosystem CO_2 exchange (NEE) with the atmosphere (Kim et al., 2012; Kimball et al., 2004; McDonald et al., 2004; Vaganov et al., 1999; Goulden et al., 1998).

Satellite radiometer and scatterometer measurements at various frequencies have been utilized to identify melt onset (Wang et al., 2013; Mortin et al., 2012) and landscape FT state (Bartsch et al., 2007; Bateni et al., 2013), but there is ambiguity in the frequency dependent response of the microwave signal to various vertical components of the soil/snow/vegetation column. While the timing of seasonal soil FT transition is closely related to the duration of seasonal snow cover (Kimball et al., 2004;

* Corresponding author.
E-mail address: chris.derksen@canada.ca (C. Derksen).

http://dx.doi.org/10.1016/j.rse.2017.03.007

Kimball et al., 2001), separating out the soil response is difficult, particularly in regions of forest vegetation (Colliander et al., 2012; Roy et al., 2015). Validation of FT state variables, be it from remote sensing products or land surface analysis (Farhadi et al., 2015) or climate models (Wang et al., 2015) is further complicated by a lack of validation sites with comprehensive, spatially distributed measurements to capture topographic, land cover, and soil related variability within a satellite sensor footprint.

The relatively recent era of spaceborne microwave measurements at L-band (1.4 GHz) have shown promise for the identification of soil FT because of the strong sensitivity to soil permittivity, which is predominantly influenced by the phase of water, coupled with greater penetration depth through vegetation and into the near surface soil than at higher (e.g. Ku/Ka-band) frequencies from sensors such as SSM/I and AMSR-E (Watanabe et al., 2011). Measurements with ground-based L-band radiometers have shown strong sensitivity to the surface FT state (Schwank et al., 2004; Rautiainen et al., 2012, 2014), with algorithms successfully scaled to satellite measurements from the ESA Soil Moisture and Ocean Salinity (SMOS) mission (Rautiainen et al., 2016; Roy et al., 2015). The passive nature of the measurement has necessitated the use of ancillary air temperature information to mitigate obviously false freeze and thaw retrievals (Rautiainen et al., 2016), while the relatively coarse spatial resolution (~50 km for SMOS; 36 km for SMAP) adds an additional challenge. High resolution L-band radar measurements from PALSAR have been utilized to effectively show local scale variability in FT transitions (Podest et al., 2014; Du et al., 2014), however the narrow swath and associated long revisit time means the data are not suitable for synoptically sensitive hemispheric FT monitoring. Data from the NASA SAC/D Aquarius mission provided the initial opportunity to determine the continental scale L-band radar response to landscape FT (Xu et al., 2016), but these measurements were constrained by very coarse spatial (~100 km) and temporal (weekly) resolutions.

The NASA Soil Moisture Active Passive (SMAP) mission, launched in January 2015, provided the first high resolution (1 to 3 km L1 high resolution radar backscatter product; resolution depends on location within the radar swath) L-band radar measurements combined with a ~1000 km swath for near daily coverage of the northern hemisphere land areas which undergo annual FT transitions. Coincident L-band measurements are also acquired at ~40 km resolution from the SMAP radiometer. One of the baseline SMAP mission objectives was to provide estimates of surface binary FT state for the region north of 45°N latitude with a classification accuracy of 80% at 3-km spatial resolution and 2-day average intervals. These measurement requirements were achieved through use of the SMAP radar measurements (Derksen et al., 2015). Unfortunately, the SMAP radar lost transmitting function in July 2015, limiting the time series of L-band radar backscatter observations to only 12 weeks (14 April through 7 July). In the event of a failure of the SMAP radar data stream, the pre-launch plan was to shift FT data production to SMAP L-band radiometer brightness temperature (T_b) measurements. An obvious compromise of this change is the coarser spatial resolution (36 km) of the T_b retrievals. The impact of changing from active to passive measurements is an open question. To address this, the overall objective of this paper is to compare the sensitivity of L-band radar measurements to the landscape FT state with coincident SMAP radiometer T_b measurements in order to determine changes in FT retrieval uncertainty between radar and radiometer based classifications. A unique set of surface measurements from an international network of in situ monitoring sites is utilized to evaluate relationships between SMAP and in situ measurement based freeze/thaw estimates.

2. Data

2.1. SMAP measurements

The SMAP spacecraft is in a 685-km circular, sun-synchronous orbit, with equator crossings at 6 AM and 6 PM local time. The radar and radiometer subsystems share a single feedhorn and parabolic mesh reflector. The radar operated with VV, HH, and HV transmit-receive polarizations with separate transmit frequencies for the H (1.26 GHz) and V (1.29 GHz) polarizations. The radiometer continues to operate, with polarizations V, H, and the third and fourth Stokes parameters, T3, and T4, at 1.41 GHz. The reflector is offset from nadir and rotates about the nadir axis at 14.6 rpm, providing a conically scanning antenna beam at a surface incidence angle of 40°. The reflector diameter is 6 m, providing a radiometer footprint of approximately 40 km (root-ellipsoidal area) defined by the one-way 3-dB beamwidth. The two-way 3-dB beamwidth defines the real-aperture radar footprint of approximately 30 km. The real-aperture (low resolution) swath width of 1000 km provides global coverage within 3 days or less equatorward of 35°N/S and 2 days poleward of 55°N/S.

To obtain the desired high spatial resolution, the radar employed range and Doppler discrimination to yield spatial resolution enhancement to 1–3 km over the 70% outer regions of the 1000-km swath. Due to data volume limitations, high-resolution radar measurements were acquired over global land areas (extending one swath width over the surrounding oceans) only during the morning (descending) overpass. During the evening (ascending) overpass, high resolution data were only collected poleward of 45°N to support diurnal landscape freeze/thaw retrievals.

2.1.1. L1C backscatter

Inputs to the SMAP Level 3 radar derived freeze/thaw product (L3_FT_A) are high resolution (L1C_S0_HiRes) SMAP radar backscatter measurements (West et al., 2016). These were acquired at 3-km resolution for the global land surface for AM (descending) orbital nodes and regions north of 45°N for PM (ascending) orbits. High resolution coverage from both orbits was limited to regions north of 45°N to support diurnal FT retrievals for regions with cold temperature constraints to ecosystem productivity and hydrological processes.

2.1.2. L1C brightness temperature

Given the failure of the SMAP radar in July 2015, the L3_FT_A algorithm will be adapted to produce landscape FT state information from SMAP L1C_TB brightness temperature measurements at a spatial resolution of 36 km. In this study, SMAP v3 L1C_Tb data were compared to SMAP high resolution radar measurements during the overlap period in spring 2015. The L1C_TB data are calibrated, geolocated, time-ordered brightness temperatures in EASE-Grid 2.0 projection format (Chan et al., 2016).

2.2. Other hemispheric FT datasets

Other datasets provide an opportunity to compare FT spatial patterns and time series information. This includes other L-band radar and radiometer measurements from Aquarius, higher frequency AMSR2 retrievals, and land surface model derived estimates.

FT information using L-band radar and radiometer measurements from the Aquarius mission were derived using a seasonal threshold approach as described in Xu et al. (2016). Also at L-band, the Aquarius measurements are much coarser spatially (~100 km), and infrequent temporally (weekly averages) compared to the SMAP data. Daily FT state from higher frequency Advanced Microwave Scanning Radiometer-2 (AMSR-2) Ka-band measurements at 25-km resolution were utilized using the dataset described in (Kim et al., 2014). The AMSR2 retrievals were derived using a seasonal threshold algorithm with pixel-wise FT references calibrated against global surface air temperature reanalysis data. The difference in frequency from SMAP introduces differences in sensitivity/penetration at the surface related to variables such as snow cover and vegetation. Finally, FT state was derived from daily averages of the top simulated soil layer (0 to 10 cm) and skin temperature from the NASA Global Model and Assimilation Office (GMAO) Goddard Earth Observing System Model, Version 5 (GEOS-5) ensemble-based land data assimilation system (Tsurf) (Reichle et al., 2016). The

Table 1
Summary of core validation sites used for SMAP radar derived freeze/thaw analysis.

Site	Cal/Val Partner	Lat	Lon	Area	IGBP land cover	Sub-grid sites
Saariselka	J. Pulliainen, Finnish Met. Insitute	68.38	27.42	Finland	Grasslands	4
Imnavait	E. Euskirchen, U. Alaska - Fairbanks	68.62	−149.30	Alaska, USA	Barren/Sparse	1
Cambridge Bay	A. Langlois, U de Sherbrooke	69.15	−105.11	Northwest Territories, Canada	Barren/Sparse	1
Baie-James	A. Royer, U de Sherbrooke	53.41	−75.01	Quebec, Canada	Coniferous Forest	2
Trail Valley Creek	P. Marsh, WLU	68.69	−133.70	Northwest Territories, Canada	Barren/Sparse	3
Chersky	M. Loranty, Colgate U	68.75	161.48	Eastern Siberia	Deciduous Needleleaf Forest	6
BERMS old black spruce	A. Black, UBC	53.99	−105.18	Saskatchewan, Canada	Coniferous Forest	2
BERMS old aspen	A. Black, UBC	53.63	−106.20	Saskatchewan, Canada	Deciduous Forest	3

combination of these two vertical layers results in a mean value that approximates the near surface soil temperature more directly than either layer individually. The GEOS-5 geophysical data are derived at a resolution of 9 km and posted on the EASE-Grid 2.0 with 9-km spacing.

2.3. In situ validation data

As outlined in the SMAP mission Calibration and Validation (Cal/Val) plan (Jackson et al., 2013) the accuracy of SMAP products are primarily determined through comparisons with in situ measurements. For FT, validation sites are located across northern latitude (≥45°N) land areas and include core (multiple sub-grid cell measurements) and sparse (single measurement point) in situ station observation networks. Because the SMAP operational record starts in early April 2015, the southern portion of the FT domain had already experienced seasonal thawing at the outset of the SMAP data record. The subset of higher latitude core validation sites used for this study is summarized in Table 1 and Fig. 1. The SMAP radar and radiometer response to the land surface FT state, and the resulting FT retrievals, were evaluated using co-located air temperature (2 m) and soil temperature (5 cm below the surface) measurements corresponding to the local time of the descending and ascending satellite overpasses (multiple measurements within a single SMAP grid cell were averaged).

The computation of the classification accuracy was derived as follows: let $s_{AM/PM}(i,t) = 1$ if the SMAP product at grid cell i and time t indicates frozen conditions for AM (descending) or PM (ascending) overpass, respectively, and let $s_{AM/PM}(i,t) = 0$ if the SMAP product indicates thawed conditions for AM or PM overpass, respectively. Likewise, let $v_{AM/PM}(i,t) = 1$ if the corresponding in situ observation (air or soil temperature are used in this study) indicates frozen conditions at the AM or PM overpass, and $v(i,t) = 0$ for thawed conditions at the AM or PM overpass. Next, the error flag δ was set by comparing the SMAP product to the validating observations:

$$\delta_{AM/PM}(i,t) = \begin{cases} 0 & if\ s_{AM/PM}(i,t) = v_{AM/PM}(i,t) \\ 1 & f\ s_{AM/PM}(i,t) \neq v_{AM/PM}(i,t) \end{cases} \quad (1)$$

The FT retrievals were separated back into binary freeze/thaw classes for the AM and PM orbits separately, producing two retrieval match-ups each day. Eq. (1) was solved daily, to provide instantaneous determinations of FT spatial accuracy, using the available reference sites. In addition to overall flag agreement, counts of freeze and thaw omission and commission errors ('false freeze' retrievals vs. 'false thaw' retrievals) are also tabulated.

3. Algorithms

3.1. Seasonal threshold approach

The SMAP baseline FT algorithm is based on a seasonal threshold approach which examines the time series progression of the remote sensing measurements relative to signatures acquired during seasonal

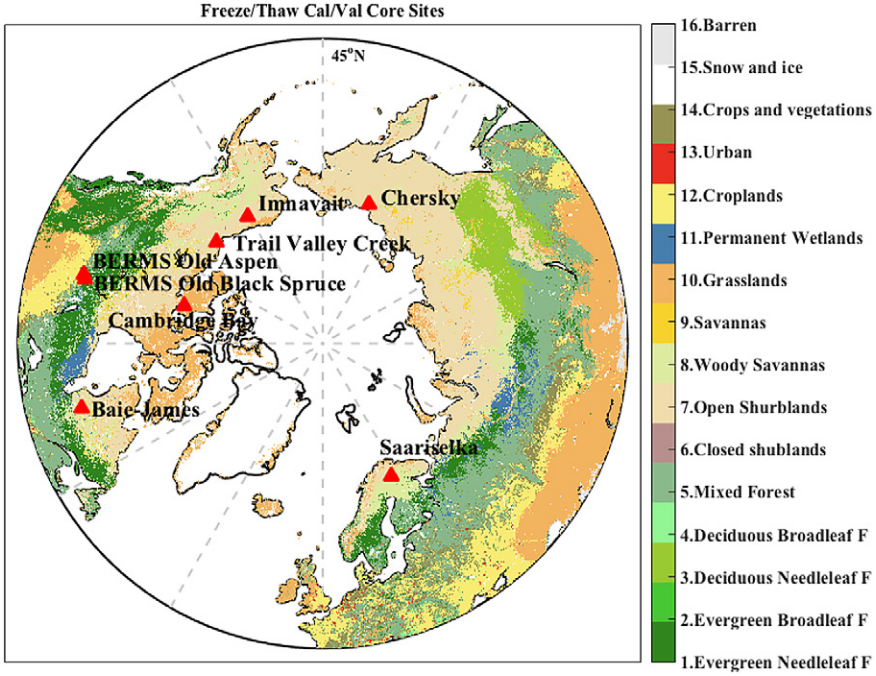

Fig. 1. Sites used for evaluation of the SMAP time series and freeze/thaw retrievals overlaid on IGBP land cover classification.

reference frozen and thawed states. In the active case, a seasonal scale factor Δ(t) is defined for an observation acquired at time *t* as:

$$\Delta(t) = \frac{\sigma(t) - \sigma_{fr}}{\sigma_{th} - \sigma_{fr}} \quad (2)$$

where $\sigma(t)$ is the measurement acquired at time *t*, for which a FT classification is sought, and $\sigma_{fr}(t)$ and $\sigma_{th}(t)$ are radar backscatter measurements corresponding to frozen and thawed reference states, respectively. A threshold level *T* is then defined such that:

$$\begin{array}{l} \Delta(t) > T \\ \Delta(t) \leq T \end{array} \quad (3)$$

defines the thawed and frozen landscape states, respectively.

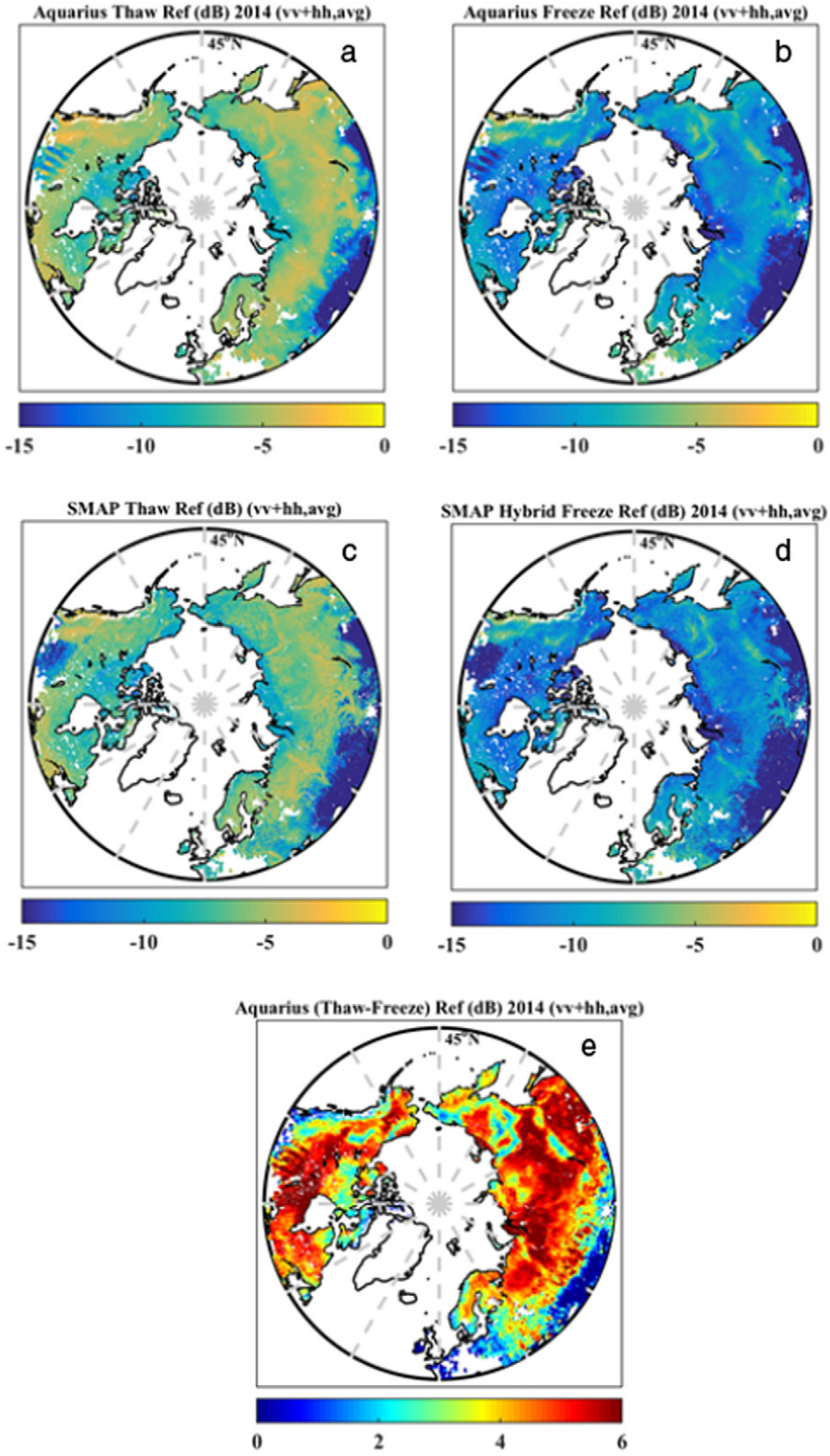

Fig. 2. Pre-launch Aquarius radar (a) thaw and (b) freeze references; final (c) SMAP thaw and (d) SMAP/Aquarius hybrid freeze reference; (e) Aquarius reference difference. Units are dB in all panels.

The same seasonal threshold algorithm is applied in the passive case. Instead of backscatter inputs, normalized polarization ratio (FF_{NPR}) is calculated from the SMAP radiometer measurements:

$$NPR = \frac{TBV - TBH}{TBV + TBH} \quad (4)$$

Decreases and increases in FF_{NPR} are associated with landscape freezing and thawing transitions, respectively, with the decrease in FF_{NPR} under frozen conditions the result of small increases in the V-pol brightness temperature combined with larger increases at H-pol (Rautiainen et al., 2012).

3.2. Freeze and thaw references

A major component of the SMAP radar baseline algorithm development involved application of existing satellite L-band radar measurements from the Aquarius mission over the FT domain to develop 100-km resolution reference maps of σ_{th}, and σ_{fr}. These pre-launch references were derived as the average of the 10 lowest (freeze) and 10 highest (thaw) ranked seasonal backscatter values for summer 2015 and winter 2015 (following Xu et al., 2016; Fig. 2a and b). Although an incidence angle correction was performed, there are still some apparent swath artifacts in the Aquarius data, particularly over the central prairies of North America.

The Aquarius radar FT references were replaced through post-launch derivation of refined FT references that included SMAP measurements. The final thaw reference (σ_{th}; Fig. 2c) for each grid cell was computed as an average over the last ten days of SMAP radar data (27 June through 6 July 2015):

$$T_{ref} = \frac{1}{n}\sum_{i=1}^{n}(\sigma_w + \sigma_{hh}), \quad n = 10 \quad (5)$$

More spatial heterogeneity can be seen in the final SMAP thaw reference (Fig. 2c) because of the finer (3 km) resolution of the SMAP radar relative to Aquarius. A direct SMAP freeze reference could not be derived as in the thaw case because no cold season SMAP radar measurements were acquired. However, based on the assumption that the thaw reference difference between SMAP and Aquarius was consistent with the freeze case, the thaw reference difference between SMAP and Aquarius was applied on a grid cell by grid cell basis as a form of post-launch bias correction to the pre-launch Aquarius freeze reference (σ_{fr}; Fig. 2d):

$$F_{ref} = F_{AQref} - (T_{AQref} - T_{ref}) \quad (6)$$

By including SMAP measurements in the derivation of a hybrid freeze reference, the artifacts in the Aquarius freeze reference (evident in Fig. 2b) were removed. Fig. 2e shows the thaw (summer 2015) versus

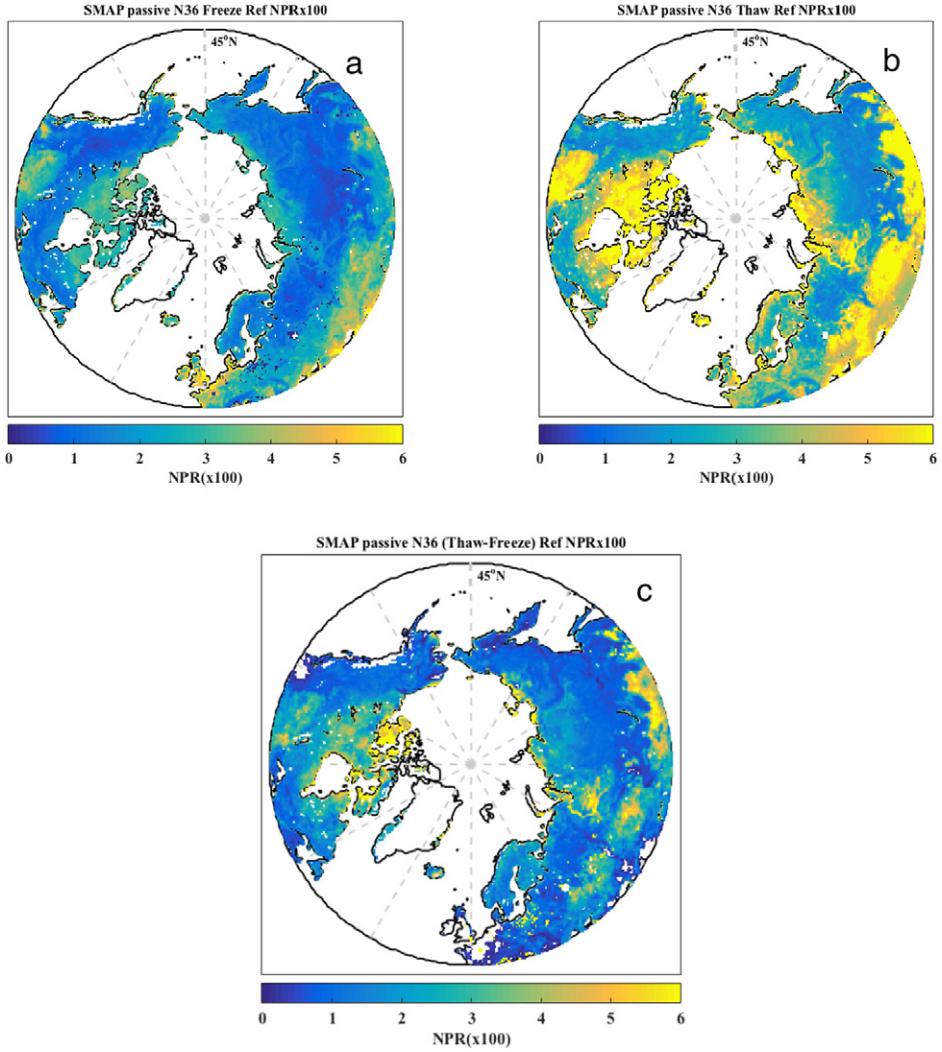

Fig. 3. SMAP radiometer (a) freeze and (b) thaw references; (c) reference difference between panels (a) and (b). Units are NPR scaled by 100.

freeze (winter 2015) reference difference from Aquarius data. There are some regions near the 45°N latitude limit, particularly in western Europe, where reference differences were below the approximately 1.5 dB threshold which limits the ability to distinguish frozen versus thawed ground from the radar signal.

The same strategy was followed for developing references for the passive freeze/thaw retrieval, with NPR replacing backscatter. SMAP derived references from the 10 highest NPR values during July and August 2015 and the 10 lowest NPR values during January and February 2016 are shown in Fig. 3a and b. Unlike the radar, SMAP radiometer measurements are available during both thaw and freeze reference periods, so the hybridization step in Eq. (6) was not necessary in the passive case. The SMAP reference differences are shown in Fig. 3c. The NPR reference differences are generally weaker than the radar case (see Fig. 2e) which indicates weaker freeze versus thaw signal to noise for the radiometer measurements. Regions with a weak NPR difference between reference freeze and reference thaw states pose a challenge to seasonal threshold algorithms, and if the reference difference gets too small, the use of ancillary surface temperature data to force the retrieval will be necessary (i.e. Rautiainen et al., 2016).

In Fig. 4, we compare the reference difference for the active versus passive cases for 13 IGBP land cover classes. In the active case, the dielectric change of the vegetation freeze/thaw state is reflected in the backscatter reference differences of 3–5 dB, even for forested land cover. However, for the passive case, forest vegetation behaves as an attenuation layer, resulting in much smaller reference differences as reflected in Fig. 3e.

3.3. Freeze/thaw retrievals

The SMAP FT algorithm is run on a grid cell-by-cell basis. The output from Eqs. (2) and (3) is a dimensionless binary state variable designating either frozen or thawed state for each unmasked grid cell (no-data flags are associated with masked surface types: ocean and inland open water, permanent ice and snow, and urban areas). The FT retrieval quantifies the predominant frozen or non-frozen status of the landscape within a grid cell and does not distinguish among different elements within the sensor footprint, including vegetation, snow cover, open water or soil conditions. While threshold optimization is possible, the parameter T is fixed at 0.5 across the entire FT domain. Full details on the L3_FT_A product can be found in the Algorithm Theoretical Basis Document (Dunbar et al., 2016).

The L3_FT_A algorithm is applied to the total power radar data: the sum of HH, VV, and HV polarized backscatter. This provides the best signal-to-noise from the SMAP radar. The L3_FT_A product uses both AM and PM high resolution data over unmasked land areas north of 45°N, posted to 3-km resolution global and north polar EASE-Grid 2 projections. The daily temporal compositing process is performed on the 3-km EASE grid data, retaining the freeze/thaw state associated with those acquisitions closest to 6:00 AM local time (AM daily product)

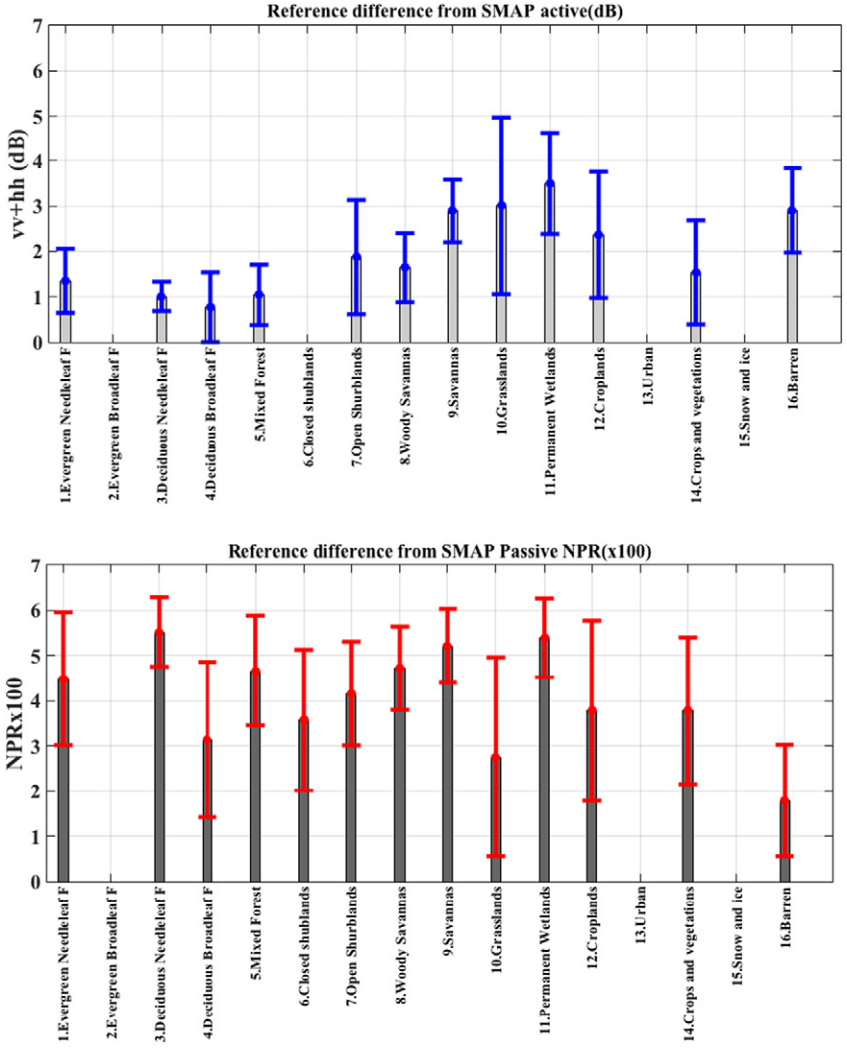

Fig. 4. (Top) SMAP reference differences for the active (dB) and (bottom) passive (NPR) cases over 13 land cover classes north of 45°. Coloured vertical lines indicate ±1 standard deviation. (For interpretation of the references to colour in this figure legend, the reader is referred to the web version of this article.)

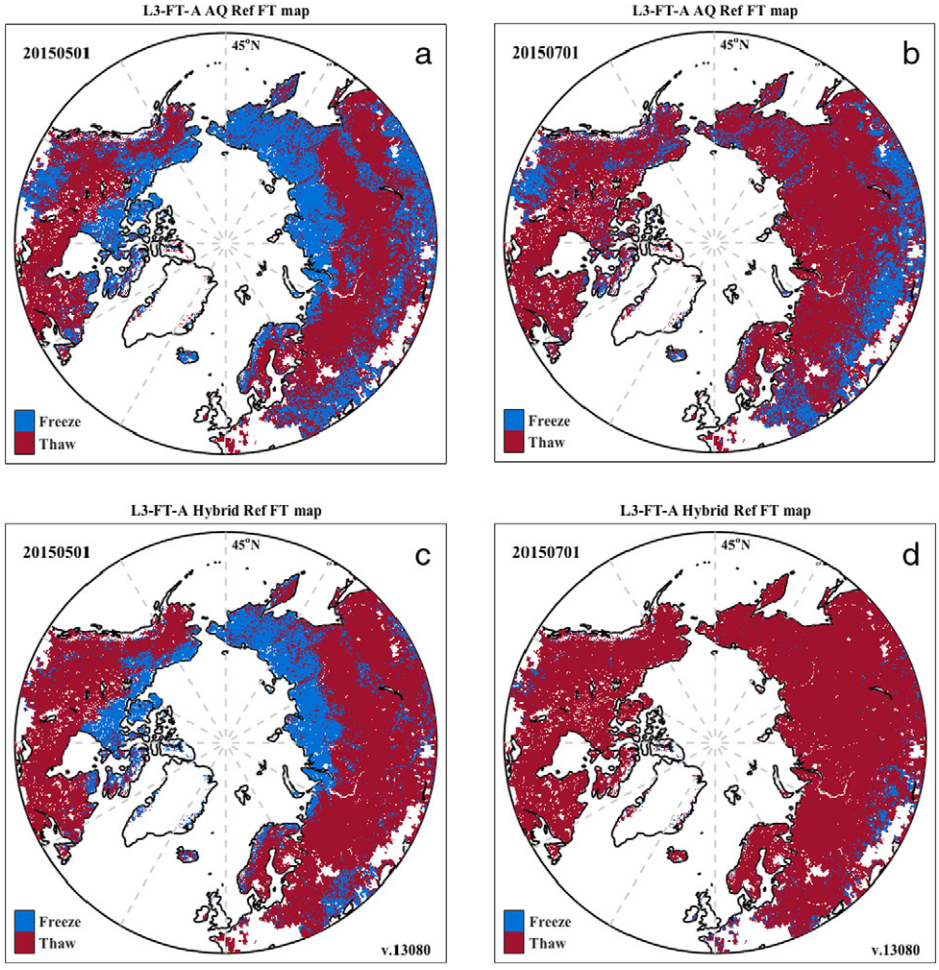

Fig. 5. Example radar FT images for 1 May 2015 (left column) and 1 July 2015 (right column) derived using: (a and b) pre-launch Aquarius references; (c and d) SMAP radar derived thaw and hybrid SMAP-Aquarius freeze references.

and 6:00 PM local time (PM daily product) of the satellite overpasses. The respective date and time of acquisition of each of the AM and PM components of the data stream is maintained in the data set. The daily L3_FT_A product thus incorporates data for the current day, as well as past days information (to a maximum of 3 days, necessary only near the southern margin of the FT domain) to ensure complete coverage of the FT domain in each day's product.

In the beta (v2) release of the L3_FT_A product, nadir track radar measurements (~150 km on either side of the nadir track) were excluded from FT processing due to uncertainties in the sensor footprint area calculations. Improvements in the L1C_S0 processing between the beta and validated (v3) product release allowed a larger proportion of the near-nadir swath to be included in the L3_FT_A release utilized in this study (only 50 km on either side of the nadir track were excluded),

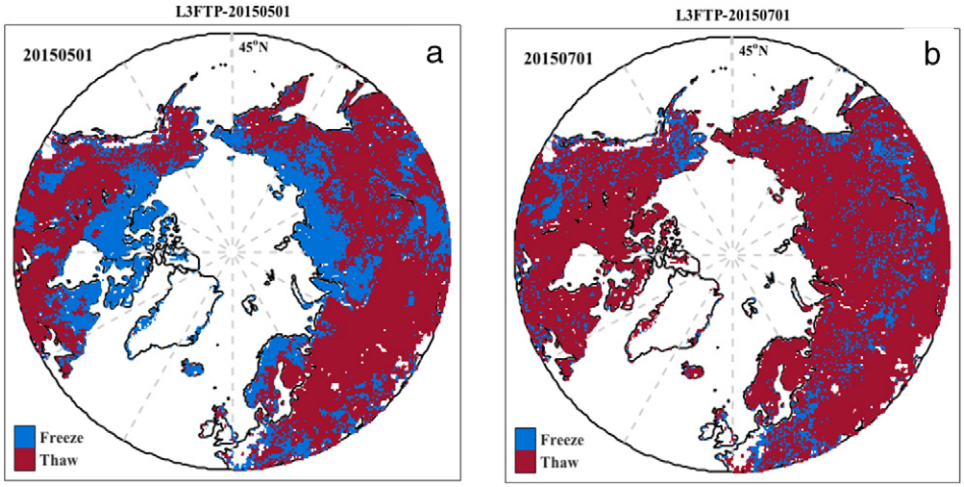

Fig. 6. Example radiometer FT images for (a) 1 May 2015, and (b) 1 July 2015.

which improves the latency of measurements utilized to maintain complete daily coverage of the FT domain. The baseline L3_FT_A algorithms do not utilize other ancillary data during execution and processing. The validated release (v3) of the SMAP L3_FT_A product (Dunbar et al., 2016) is available from the National Snow and Ice Data Center (NSIDC), and is derived from Version 3 of the L1C_S0 dataset (available from the Alaska Satellite Facility) (West et al., 2016).

The L3_FT_P algorithm is applied to NPR values calculated from regridded L1C_TB radiometer data (Chan et al., 2016). As in the radar case, the intermediate orbit-specific freeze/thaw products are temporally composited to assemble freeze/thaw state maps separately for AM and PM acquisitions. The final daily L3_FT_P product is posted to both polar and global equal-area Earth grids. Archive and distribution via NSIDC is forthcoming.

4. Results

The objective of this study is not to focus solely on retrieval agreement statistics with respect to the 80% spatial accuracy target established by the mission. Instead, the aim is to compare the SMAP radar and radiometer response to the surface state in order to both document the quality of the short time series of the SMAP radar FT product, and compare the passive sensitivity to surface FT state in advance of the release of a SMAP radiometer FT product.

4.1. Large scale patterns and features

Example SMAP radar derived FT maps generated using the prelaunch Aquarius references and final SMAP references (see Section 3) are shown in Fig. 5. While resulting differences in the classified frozen area are small, the use of SMAP references result in a notable reduction in clearly erroneous false freeze retrievals across high elevation areas and the southern portion of the FT domain in July. This improvement is particularly clear by July, when the entire FT domain was essentially thawed. The remaining false freeze flags apparent across the southern portion of the FT domain are in large part due to small freeze versus thaw reference differences in Fig. 2e, and can be removed using conservative air temperature screening from, for example, reanalysis products. Overall, Fig. 5 shows clean algorithm performance with spatially coherent retrievals and no processing artifacts.

Radiometer derived FT maps for the same two dates are shown in Fig. 6. The frozen area retrievals across northern latitudes on 1 May 2015 are similar to the radar retrievals in Fig. 5. The false freeze retrievals remain an issue, but occur across different spatial regions than the radar derived false freeze flags. This indicates the regions with poor freeze versus thaw signal to noise differ between the backscatter and NPR measurements.

4.2. Radar and radiometer time series from core sites

Fig. 7 shows time series of descending overpass SMAP measurements with coincident air and soil temperature measurements (5 cm depth), from 1 April–7 July 2015 (initial date of SMAP radiometer science data through final day of SMAP radar science data) from the five core validation sites that clearly transitioned from frozen to thawed states during this period. Horizontal coloured lines denote the period of frozen conditions, determined either as a retrieval from SMAP measurements (radar; radiometer) or from the in situ temperature measurements. Horizontal dashed lines indicate radar backscatter and NPR freeze and thaw reference values utilized for the seasonal threshold algorithm retrieval. In general, there is agreement in time between the radar backscatter and radiometer NPR values, with the range in correlations illustrated in Fig. 8. Pre-launch assessments indicated that L-band radar measurements would deliver a 3 to 5 dB signal response to FT. A response within this magnitude range is evident at these core sites. The magnitude of NPR response is variable, however, with muted values at Chersky and Trail Valley Creek, but very strong peaks associated with melt onset at Cambridge Bay and Imnavait.

An additional difference in the backscatter versus NPR response is the behaviour of the signal following the primary spring thaw transition. While the radar backscatter remains at elevated values relative to the frozen state, the NPR tends to drift downwards following the main thaw transition (de-polarization of the scene). Imnavait provides a clear example of this, with a spike in NPR corresponding to the primary transition followed by a gradual decline in NPR, which eventually falls below the threshold value in late June, triggering false freeze flags.

There is evidence that the SMAP FT flags are responding to the onset of wet snow cover conditions because the end of the frozen period in the retrievals occurs with the arrival of persistent warmer surface air temperatures above the freezing point (~0 °C) of liquid water and consistent with the onset of spring snowmelt; however, soil temperatures lag behind the increase in surface air temperatures and remain at or below freezing until the snowpack is depleted. This relationship with air temperature is further illustrated in Fig. 8, with stronger correlations in comparison to soil temperature. Late spring ephemeral re-freeze periods identified from the surface air temperature measurements coincide with a decrease in radar backscatter and NPR, but the response is not always sufficiently strong to drop the values below the FT threshold. For example, late season re-freezing was captured at Imnavait, but not Trail Valley Creek.

The potential benefits of future threshold optimization are evident at the Saariselka site in Finland. Conditions at this site were nominally frozen at the beginning of April with air temperatures below freezing, although soil temperatures were near zero due snow insulation. Following a period of colder temperatures in mid-April, backscatter decreased, but did not fall below the FT threshold value, resulting in no frozen retrievals. NPR values oscillated around the FT threshold, producing intermittent frozen and thawed retrievals. An optimization of the radar FT threshold to a higher value would result in consistently frozen retrievals at this site during April, in agreement with in situ measurements.

A comparison of spatial maps between Figs. 5 and 6, and the time series of radar backscatter and NPR values at the five sites illustrated in Fig. 7 are encouraging with respect to the transition to a radiometer based retrieval with similar performance characteristics to the radar. The transition from frozen to thawed states produced a NPR response similar in timing and magnitude to the backscatter response, resulting in similar dates of the primary freeze to thaw transition event (Fig. 9). This suggests the retrieval challenge in the passive case is not in the magnitude of the response in NPR during the FT transitions, but rather the stability/variability of NPR particularly during the summer.

At the other core validation sites, the spring transition from frozen to thawed states was already underway at the onset of SMAP measurements in April 2015. These sites are illustrated in Fig. 10, and show the clear benefit of the diurnal measurement capabilities of SMAP. At the James Bay site, the primary thaw transition occurred in early April when SMAP radiometer, but no radar measurements, were available due to different commissioning schedules for the two instruments. The apparent thaw transition is captured in the NPR time series for both orbits, but warmer conditions occurring during the afternoon orbits are evident in the higher NPR values. This is also the case at the BERMS old black spruce site. Interestingly, despite the coarse spatial resolution, the radiometer measurements capture diurnal and ephemeral freeze/thaw events better than the radar at these two sites although some of this may be related to the quality of the radar freeze references (for the passive case, both the thaw and freeze references come directly from SMAP measurements, while no SMAP freeze reference was available for the radar case).

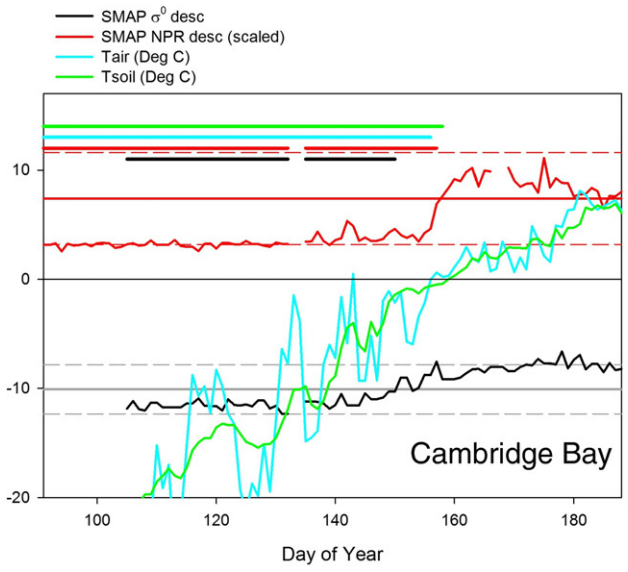
SMAP σ⁰ desc
SMAP NPR desc (scaled)
Tair (Deg C)
Tsoil (Deg C)
Cambridge Bay
Day of Year

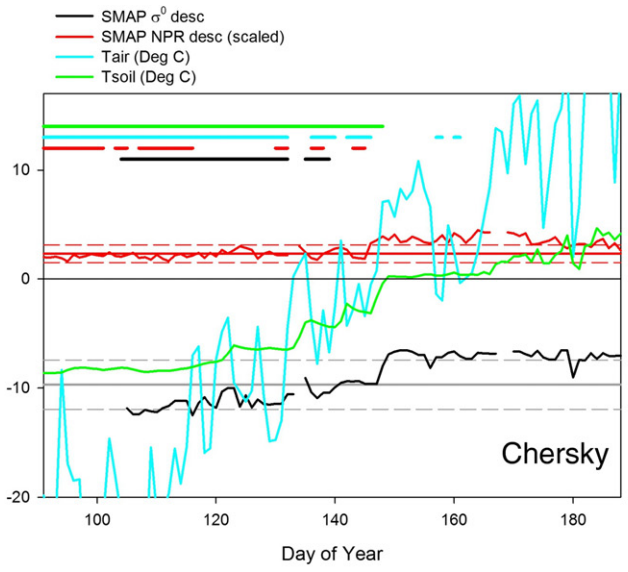
SMAP σ⁰ desc
SMAP NPR desc (scaled)
Tair (Deg C)
Tsoil (Deg C)
Chersky
Day of Year

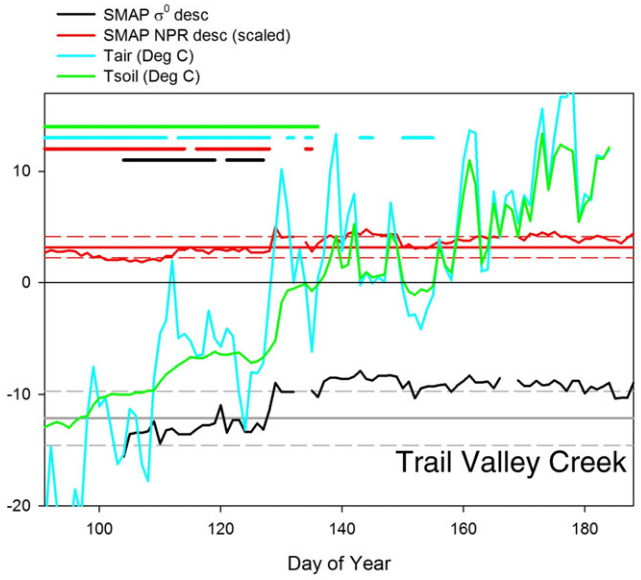
SMAP σ⁰ desc
SMAP NPR desc (scaled)
Tair (Deg C)
Tsoil (Deg C)
Trail Valley Creek
Day of Year

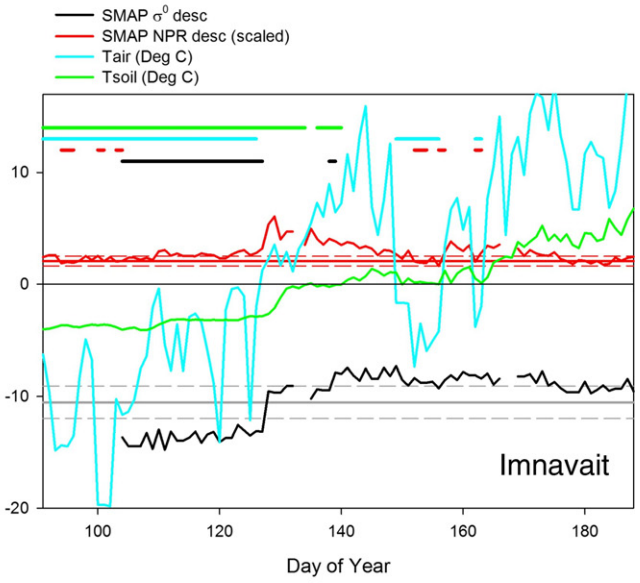
SMAP σ⁰ desc
SMAP NPR desc (scaled)
Tair (Deg C)
Tsoil (Deg C)
Imnavait
Day of Year

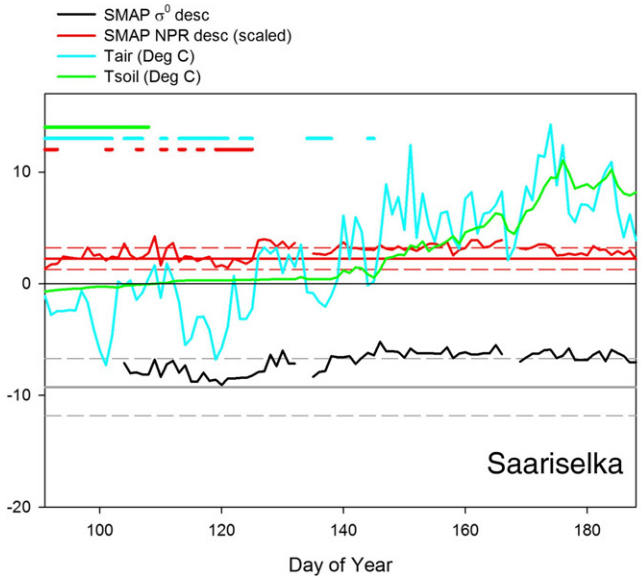
SMAP σ⁰ desc
SMAP NPR desc (scaled)
Tair (Deg C)
Tsoil (Deg C)
Saariselka
Day of Year

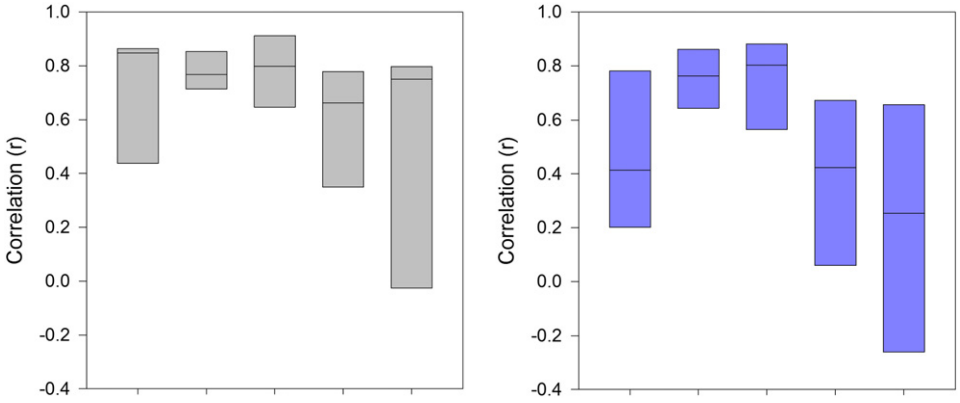

Fig. 8. Boxplots of correlations at core validation sites that transitioned from freeze to thaw during the SMAP radar data period (see Fig. 7) for descending (left) and ascending (right) overpasses (σ^0 = backscatter; NPR = normalized polarization ratio; Tair = surface air temperature; Tsoil = near surface soil temperature).

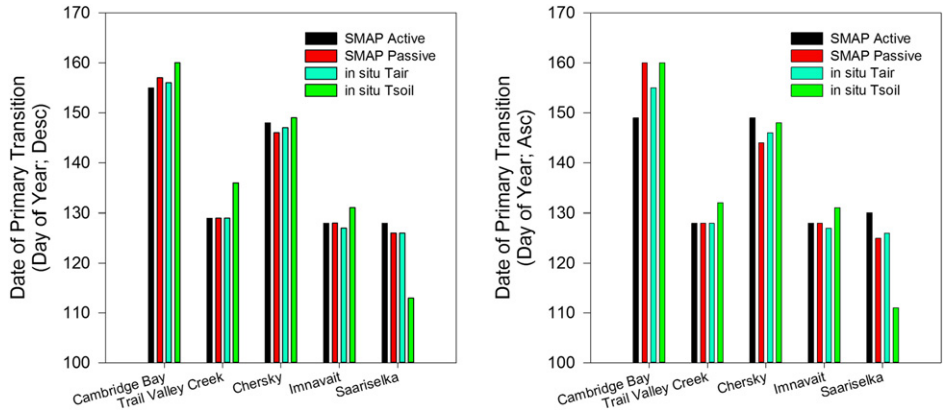

Fig. 9. Date of primary freeze to thaw transition.

4.3. Product validation results

Fig. 11 shows the FT flag agreement values between SMAP and the in situ measurements during the period of overlapping SMAP radar and radiometer measurements for the sites in Figs. 7 and 10. Multiple sources of uncertainty influence these agreement statistics. First, there is a tendency for the FT retrievals to transition to thawed conditions when surface air temperatures increase above freezing (0.0 °C) but soil temperatures remain below zero presumably due to the influence of wet snow on the SMAP signal (Du et al., 2014). This results in better agreement during the early transitional period when air temperature is used as the validation reference. Conversely, there is a tendency for ephemeral re-freeze events to be missed by the SMAP FT retrievals because they induce an insufficiently strong response in the backscatter or NPR values. This will produce higher disagreement with air temperature flags because soil temperatures respond much more slowly to air temperature forcing, and so remain thawed during these short periods in spring when air temperatures drop back below zero for short periods of time.

Overall, better FT agreement between SMAP retrievals and in situ validation data was obtained for ascending versus descending orbits, but there is no clear performance difference between the use of air versus soil temperature as the validation metric because of the competing effects described above. The relatively similar overall performance of the retrievals compared to soil versus air temperature may be a function of melt processes at these sites. Melt onset was rapid at Cambridge Bay, Imnavait, and Trail Valley; with a relatively thin tundra snow pack, there is a short offset between air temperatures and soil temperatures rising above zero.

To further diagnose retrieval performance, error matrices for two example sites are shown in Tables 2 and 3, for both air and soil temperature based FT validation references. The results for Trail Valley Creek (Table 2) are illustrative of the sites that transitioned from frozen to thawed conditions during the SMAP radar period. The tendency for the SMAP retrievals to classify spring thaw onset slightly before the thaw transition of the soil temperature reference flags (note values in the yellow cells in Table 2) indicates backscatter and NPR response to the onset of wet snow cover. These false thaw retrieval errors are higher for the morning overpasses because the reference flags capture diurnal refreeze in the morning, but return to a thawed state (and hence agreement with the retrieval) by the afternoon overpass. Some false freeze events (blue cells in Table 2) are apparent during the afternoon overpasses, again related to diurnal thaw events, which the SMAP measurements did not detect. In general, the error characteristics for these types of sites are very similar for active and passive cases, and for the use of air and soil temperature reference flags, respectively.

The James Bay site (Table 3) is illustrative of sites that did not undergo a clean transition from frozen to thawed states during the period of SMAP radar operation. These error matrices show clear differences

Fig. 7. Time series of descending overpass SMAP measurements with coincident air and soil temperature, from 1 April – 7 July 2015 (initial date of SMAP radiometer science data through final day of SMAP radar science data) for core validation sites that transitioned from freeze to thaw during this period. Horizontal coloured lines denote estimate of frozen conditions. Gray dashed lines indicate backscatter freeze and thaw reference values; red dashed lines indicate NPR references. (For interpretation of the references to colour in this figure legend, the reader is referred to the web version of this article.)

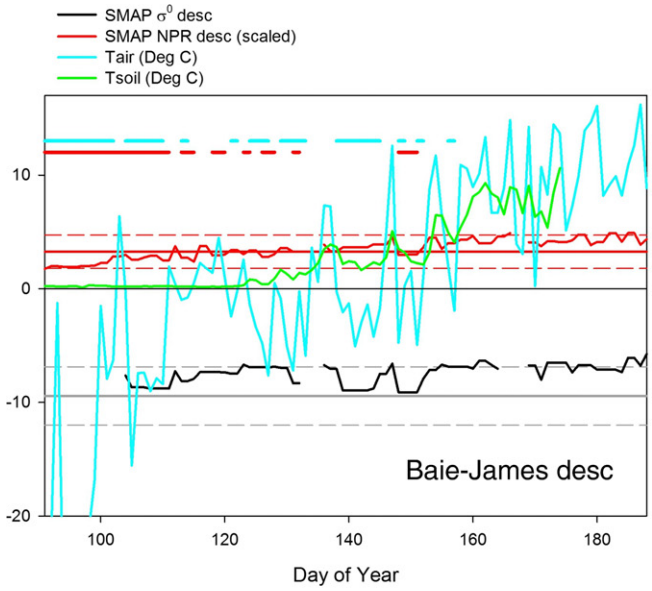
SMAP σ⁰ desc
SMAP NPR desc (scaled)
Tair (Deg C)
Tsoil (Deg C)
Baie-James desc
Day of Year

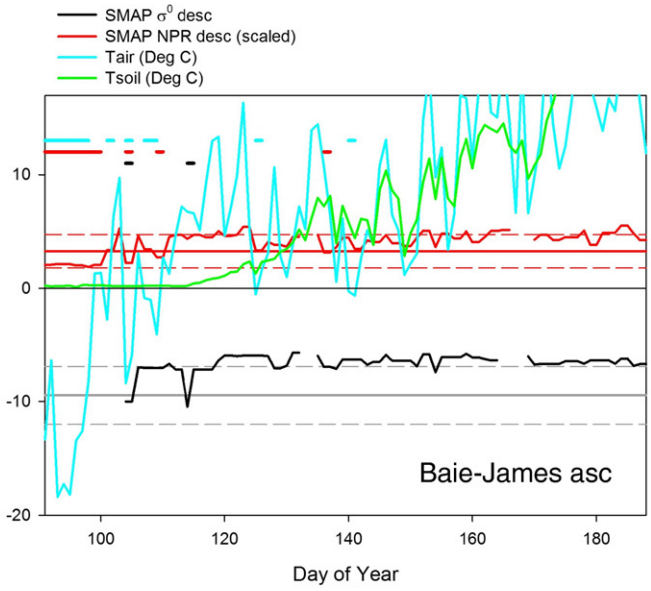
SMAP σ⁰ desc
SMAP NPR desc (scaled)
Tair (Deg C)
Tsoil (Deg C)
Baie-James asc
Day of Year

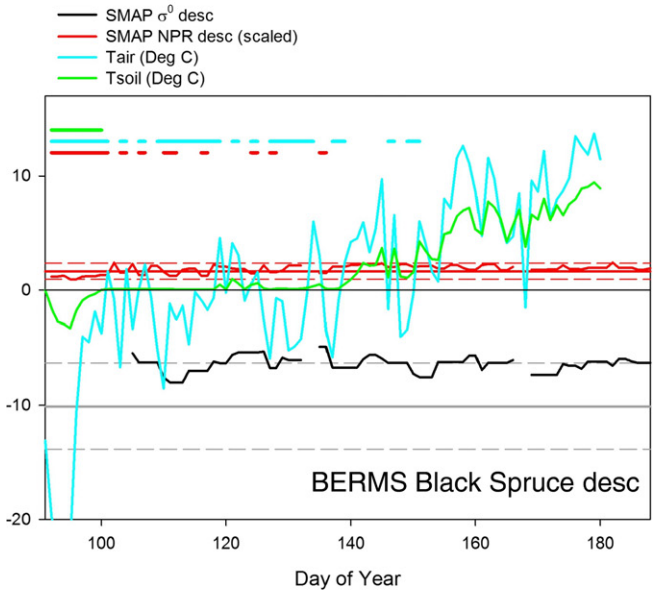
SMAP σ⁰ desc
SMAP NPR desc (scaled)
Tair (Deg C)
Tsoil (Deg C)
BERMS Black Spruce desc
Day of Year

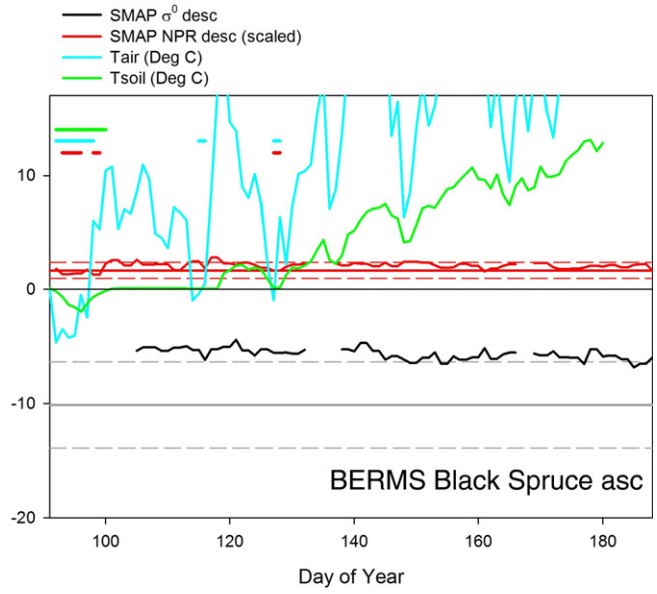
SMAP σ⁰ desc
SMAP NPR desc (scaled)
Tair (Deg C)
Tsoil (Deg C)
BERMS Black Spruce asc
Day of Year

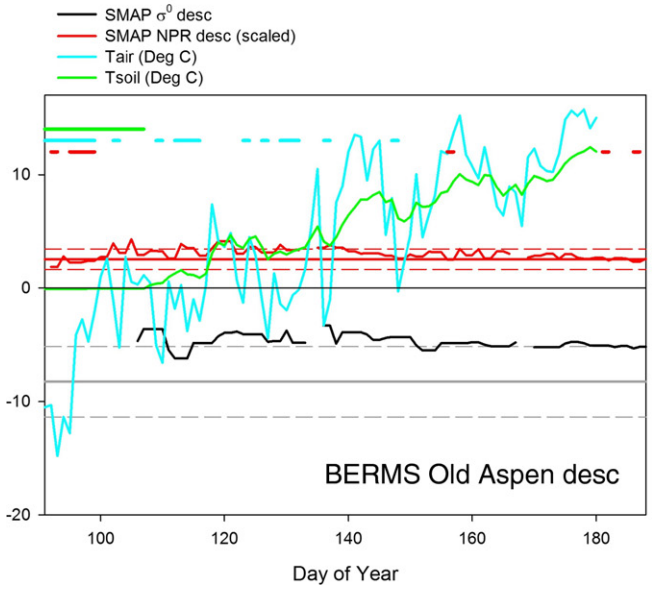
SMAP σ⁰ desc
SMAP NPR desc (scaled)
Tair (Deg C)
Tsoil (Deg C)
BERMS Old Aspen desc
Day of Year

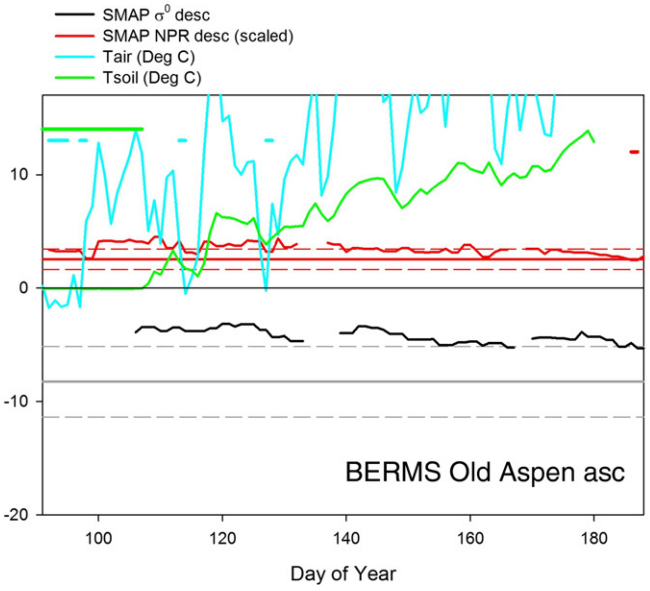
SMAP σ⁰ desc
SMAP NPR desc (scaled)
Tair (Deg C)
Tsoil (Deg C)
BERMS Old Aspen asc
Day of Year

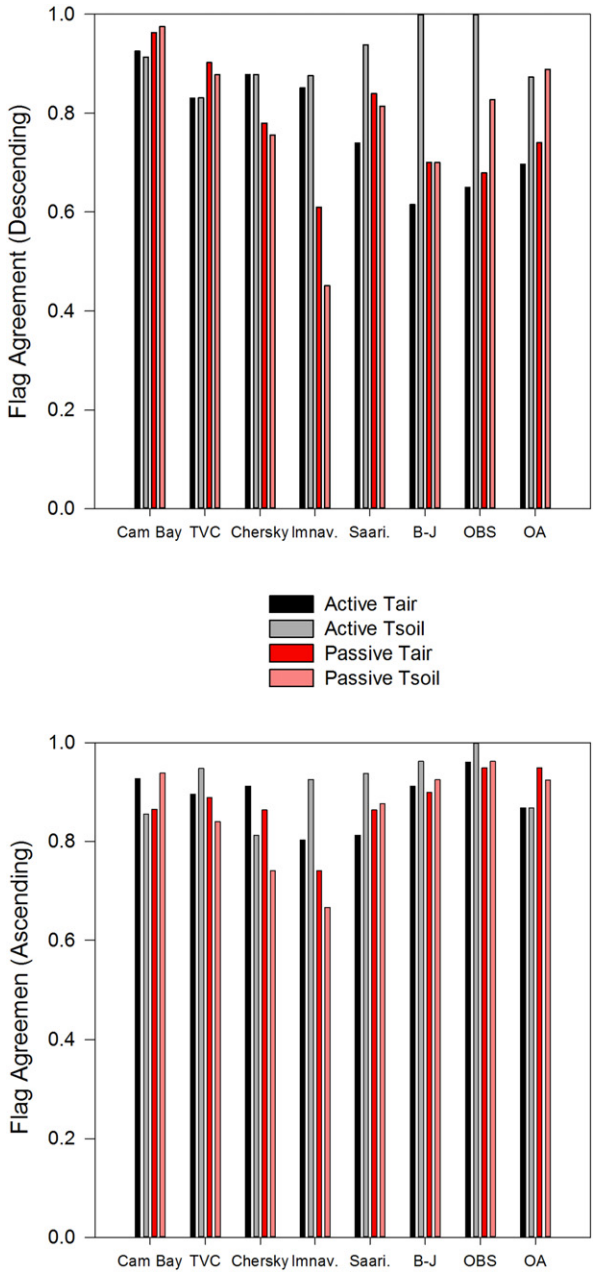

Fig. 11. Freeze/thaw flag agreement for core validation sites over the 1 April–7 July 2015 period, descending (top) and ascending (bottom) overpasses.

between overpass time and reference flag. Agreement is notably weaker for the descending orbits because of false thaw retrievals (diurnal refreezing not captured, as was the case above). These false thaw errors are only captured by the air temperature reference flag, however, because soil temperatures did not respond to such short-term forcing. As in Table 2, the error characteristics between the active and passive cases are similar.

4.4. Hemispheric frozen area time series

An example of five coincident FT estimates for 20 April 2015 is shown in Fig. 12 (note the Aquarius data cover a week centered on 20 April). While there are resolution differences (3 km for SMAP; 100 km for Aquarius; 25 km for AMSR2), all five datasets capture the same general FT pattern, with some regional differences in areas of complex

Table 2
Error matrices for Trail Valley Creek (top = radar; bottom = radiometer) Flag agreement = green cells; false freeze (SMAP = freeze, reference flags = thaw) = blue cells; false thaw (SMAP = thaw, reference flags = freeze) = yellow cells.

	Tair–PM–F	Tair–PM–T	Tair–AM–F	Tair–AM–T
Active–Asc–F	22%	9%		
Active–Asc–T	1%	68%		
Active–Des–F			29%	1%
Active–Des–T			16%	55%
	Tsoil–PM–F	Tsoil–PM–T	Tsoil–AM–F	Tsoil–AM–T
Active–Asc–F	31%	0%		
Active–Asc–T	5%	64%		
Active–Des–F			30%	0%
Active–Des–T			17%	53%
	Tair–PM–F	Tair–PM–T	Tair–AM–F	Tair–AM–T
Passive–Asc–F	15%	4%		
Passive–Asc–T	7%	74%		
Passive–Des–F			34%	1%
Passive–Des–T			9%	56%
	Tsoil–PM–F	Tsoil–PM–T	Tsoil–AM–F	Tsoil–AM–T
Passive–Asc–F	19%	0%		
Passive–Asc–T	16%	65%		
Passive–Des–F			34%	1%
Passive–Des–T			11%	54%

Table 3
As in Table 2 but for Baie-James.

	Tair–PM–F	Tair–PM–T	Tair–AM–F	Tair–AM–T
Active–Asc–F	3%	1%		
Active–Asc–T	8%	88%		
Active–Des–F			0%	0%
Active–Des–T			38%	62%
	Tsoil–PM–F	Tsoil–PM–T	Tsoil–AM–F	Tsoil–AM–T
Active–Asc–F	0%	4%		
Active–Asc–T	0%	95%		
Active–Des–F			0%	0%
Active–Des–T			0%	100%
	Tair–PM–F	Tair–PM–T	Tair–AM–F	Tair–AM–T
Passive–Asc–F	4%	4%		
Passive–Asc–T	6%	86%		
Passive–Des–F			19%	11%
Passive–Des–T			19%	51%
	Tsoil–PM–F	Tsoil–PM–T	Tsoil–AM–F	Tsoil–AM–T
Passive–Asc–F	0%	8%		
Passive–Asc–T	0%	93%		
Passive–Des–F			0%	30%
Passive–Des–T			0%	70%

Fig. 10. Time series of descending (left column) and ascending (right column) SMAP measurements with coincident air and soil temperature for core validation sites already transitioning between frozen and thawed states by 1 April 2015. Gray dashed lines indicate backscatter freeze and thaw reference values; red dashed lines indicate NPR references. (For interpretation of the references to colour in this figure legend, the reader is referred to the web version of this article.)

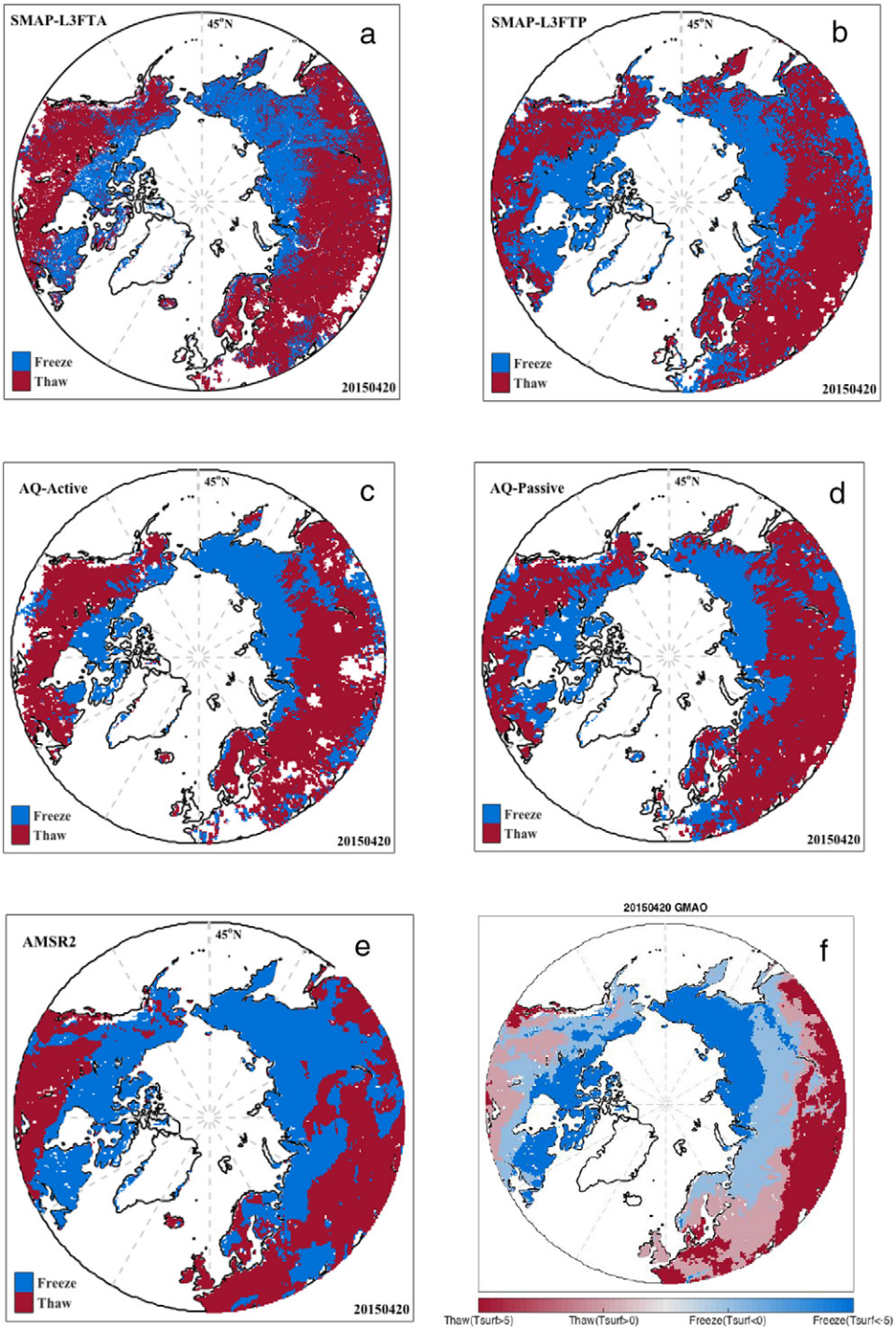

Fig. 12. Snapshot comparison (20 April 2015) of five satellite derived FT retrievals: (a) SMAP L3_FT_A; (b) SMAP L3_FT_P; (c) Aquarius active; (d) Aquarius passive; (e) AMSR2. Daily averaged FT information from GMAO Tsurf simulations are shown in (f).

elevation, and along freeze/thaw transition areas. In general, the passive products (Aquarius and AMSR2) retrieve less frozen area than the active products.

A comparison of the time series of SMAP derived frozen area across land areas north of 45° compared to Aquarius, AMSR2, and GMAO surface temperature derived estimates are shown in Fig. 13 for both overpasses. There are inter-dataset differences in the rate of areal thaw due to differences in frequency (i.e. L-band for SMAP; Ka-band for AMSR2), spatial resolution (i.e. 3 km for SMAP; 25 km for AMSR2; 100 km for Aquarius) and the sensitivity of the active versus passive measurements. An important difference between products is the timing and duration of complete summer thaw conditions. The GMAO Tsurf product shows complete thaw by early June, in close agreement with the pm overpasses of the AMSR2 product. Note that the GMAO Tsurf data were averaged daily, hence the AM and PM overpass time series in Fig. 13 are identical. The SMAP and Aquarius estimates retain a higher amount of frozen area due to false freeze flags. These false flags are more predominant in the AM overpasses. Approaches to remove these flags using a combination of climatological masks and reference calibration (as used with the AMSR2 product) are currently being developed.

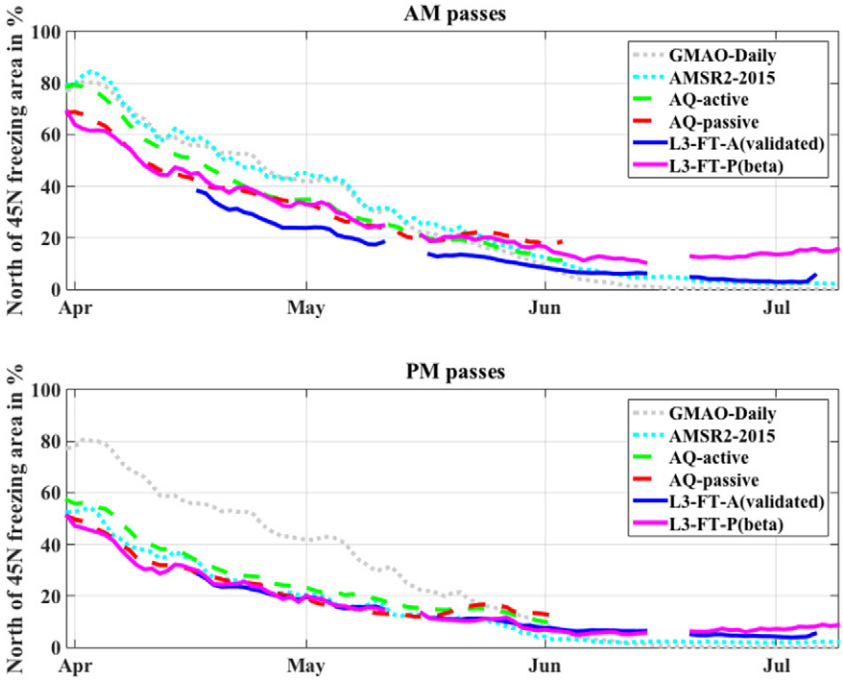

Fig. 13. Time series of % frozen area across the FT domain for AMSR-E, Aquarius radar and radiometer, and SMAP radar and radiometer datasets. Note that the GMAO Tsurf derived FT fractions are daily averaged, and hence the time series in both panels is the same.

5. Discussion and conclusions

This comparison of SMAP active and passive measurements during the period of radar operation identified very similar response to the land surface state transition from frozen to thawed. FT retrievals produced using SMAP thaw references and hybrid SMAP/Aquarius freeze references, a maximum 50% lake fraction threshold showed clean algorithm performance with spatially coherent retrievals and no apparent processing artifacts. Some false freeze flags are apparent across the southern portion of the FT domain, which can be mitigated using conservative air temperature screening incorporating ancillary data available from global reanalysis.

In general, FT retrievals are challenging to validate because the spaceborne measurement must be related to the FT state of a horizontally (land cover; topography) and vertically (soil/snow/vegetation) heterogeneous scene. There were also a limited number of sites with comprehensive measurements available for validation. Assessment at high-latitude core validation sites showed excellent agreement with in situ temperature measurement based FT reference flags, exceeding the 80% SMAP mission requirement. Similar performance was found for air temperature and soil temperature derived FT reference flags, although there was a tendency for the SMAP spring thaw signal to lead the soil temperature based FT reference flag, which was attributed to the influence of wet snow cover on the radar and radiometer signal. It is therefore important for users to understand that the satellite FT retrievals represent an integrated landscape state, not simply the near-surface soil layer. It is clear that during the spring thaw transition, both active and passive SMAP measurements responded to initial increases in air temperature above freezing, indicating sensitivity to wet snow, not soil thaw. Continued analysis of SMAP radiometer measurements will identify seasonal differences in how landscape components influence the temporal FT signal (i.e. snow free soil freeze versus snow covered soil freeze in the fall; wet snow over frozen ground in the spring).

Given the failure of the SMAP radar in July 2015 and the short measurement period, there are limited planned updates to the L3_FT_A product. Instead, a mission priority is to develop the alternative FT product using L-band radiometer brightness temperature retrievals (L3_FT_P) from the SMAP radiometer, which continues normal operations with excellent calibration accuracy and performance (Piepmeier et al., 2016). The SMAP freeze/thaw team will continue to pursue developments in the following areas:

- The original plan for L3_FT_A product updates was based on a rotating schedule of reference updates, threshold optimization, and re-processing. While this plan cannot be implemented due to the short SMAP radar time series, it is still possible to perform a threshold optimization across portions of the FT domain. Optimization experiments may be conducted at core and sparse network sites in order to determine the potential impact. Threshold optimization will also occur as part of L3_FT_P product development and validation.
- Additional validation sites will be pursued, and comparisons with other satellite derived freeze/thaw datasets (as illustrated in Figs. 12 and 13) will also be extended to include FT retrievals developed with data from the Soil Moisture Ocean Salinity (SMOS) mission (Rautiainen et al., 2016).
- Triple collocation (TC) is used within the SMAP project to validate soil moisture retrievals using sparse network observations. However, application of TC to categorical target variables such as freeze/thaw results in biased error estimates and violation of critical TC assumptions. Categorical Triple Collocation (CTC), a variant of TC that relaxes these assumptions was recently developed for application to categorical target variables such as FT (McColl et al., 2016).
- Unlike soil moisture, there is no legacy of airborne L-band remote sensing campaigns to support process studies, scaling, and algorithm development for FT. An active/passive L-band airborne freeze-thaw campaign (collaboration between NASA, Environment Canada, and Agriculture and Agri-Food Canada) was conducted during transient FT events over agricultural land in Manitoba, Canada during the first two weeks of November 2015. Analysis of this dataset will primarily support L3_FT_P development.

With the loss of the SMAP radar, FT science activities will be recovered/mitigated by using the radiometer data for passive FT retrieval. Recent analysis of SMOS and Aquarius measurements illustrates the

potential for L-band radiometer retrievals of landscape FT using a retrieval method conceptually similar to the SMAP radar retrieval (Roy et al., 2015; Rautiainen et al., 2016). Expected impacts on retrieval performance compared to L3_FT_A will likely be related to changes in sensitivity, stability, signal to noise ratio, and increased spatial classification error due to the coarser resolution (36 vs. 3 km). Efforts are also underway within the SMAP project to provide enhanced resolution radiometer measurements through the application of Backus-Gilbert resampling. The 9-km enhanced resolution brightness temperature product will feed into an enhanced FT product (L3_FT_P_E). While still coarser than the radar derived product, this intermediate resolution product should improve sensitivity to the influence of landscape heterogeneity on FT processes.

Acknowledgments

The research described in this publication was carried out in part at the Jet Propulsion Laboratory, California Institute of Technology, under a contract with the National Aeronautics and Space Administration. ML received support from the National Science Foundation PLR-1304464. Work at the Imnavait sites was funded by the National Science Foundation Division of Polar Programs Arctic Observatory Network grant numbers 0632264 and 1107892 Canadian contributions to the SMAP mission are supported by the Canadian Space Agency.

References

Bartsch, A., Kidd, R., Wagner, W., Bartalis, Z., 2007. Temporal and spatial variability of the beginning and end of daily spring freeze/thaw cycles derived from scatterometer data. Remote Sens. Environ. 106, 360–374.

Bateni, S.M., Huang, C., Margulis, S., Podest, E., McDonald, K., 2013. Feasibility of characterizing snowpack and the freeze–thaw state of underlying soil using multifrequency active/passive microwave data. IEEE Trans. Geosci. Remote Sens. 51 (7), 4085–4102.

Black, T.A., Chen, W., Barr, A., Arain, A., Chen, Z., Nesic, Z., Hogg, E., Neumann, H., Yang, P., 2000. Increased carbon sequestration by a boreal deciduous forest in years with a warm spring. Geophys. Res. Lett. 27 (9), 1271–1274.

Chan, S., Njoku, E.G., Colliander, A., 2016. SMAP L1C Radiometer Half-orbit 36 km EASE-grid Brightness Temperatures, Version 3. [Indicate Subset Used]. NASA National Snow and Ice Data Center Distributed Active Archive Center, Boulder, Colorado USA http://dx.doi.org/10.5067/E51BSP6V3KP7 (Date Accessed).

Chapin III, F., Sturm, M., Serreze, M., McFadden, J., Key, J., Lloyd, A., McGuire, A., Rupp, T., Lynch, A., Schimel, J., Beringer, J., Chapman, W., Epstein, H., Euskirchen, E., Hinzman, L., Jia, G., Ping, C., Tape, K., Thompson, C., Walker, D., Welker, J., 2005. Role of land-surface changes in Arctic summer warming. Science 310:657–660. http://dx.doi.org/10.1126/science.1117368.

Colliander, A., McDonald, K., Zimmermann, R., Schroeder, R., Kimball, J., Njoku, Eni G., 2012. Application of QuikSCAT backscatter to SMAP validation planning: freeze/thaw state over ALECTRA sites in Alaska from 2000 to 2007. IEEE Trans. Geosci. Remote Sens. 50 (2), 461–468.

Derksen, C., Xu, X., Dunbar, R.S., Colliander, A., 2015. Soil moisture active passive (SMAP) project calibration and validation for the L3_FT_A validated-release data product. Jet Propulsion Laboratory Technical Document JPL D-93721 30 pp. https://nsidc.org/sites/nsidc.org/files/files/smap/reports/SMAP%20L3_FT_A%20Validated%20Assessment%20Report%20Final.docx.

Du, J., Kimball, J., Azarderakhsh, M., Dunbar, R.S., Moghaddam, M., McDonald, K., 2014. Classification of Alaska spring thaw characteristics using satellite L-band radar remote sensing. IEEE Trans. Geosci. Remote Sens. 53 (1):542–556. http://dx.doi.org/10.1109/TGRS.2014.2325409.

Dunbar, S., Xu, X., Colliander, A., Derksen, C., McDonald, K., Podest, E., Njoku, E., Kimball, J., Kim, Y., 2016. SMAP L3 Radar Northern Hemisphere Daily 3 km EASE-grid Freeze/Thaw State. Version 3. [Indicate Subset Used]. NASA National Snow and Ice Data Center Distributed Active Archive Center, Boulder, Colorado USA http://dx.doi.org/10.5067/CPSA0M496MGB (Date accessed).

Farhadi, L., Reichle, R., DeLannoy, G., Kimball, J., 2015. Assimilation of freeze–thaw observations into the NASA catchment land surface model. J. Hydrometeorol. 16, 730–743.

Goulden, M.L., Wofsy, S., Harden, J., Trumbore, S., Crill, P., Gower, S., Fries, T., Daube, B., Fan, S., Sutton, D., Bazzaz, A., Munger, J., 1998. Sensitivity of boreal forest carbon balance to soil thaw. Science 279 (9), 214–217.

Jackson, T.J., Colliander, A., Kimball, J., Reichle, R., Crow, W., Entekhabi, D., O'Neill, P., Njoku, E., 2013. SMAP Science Data Calibration and Validation Plan. SMAP Mission. JPL. http://smap.jpl.nasa.gov/science/validation/.

Jarvis, P., Linder, S., 2000. Constraints to growth of boreal forests. Nature 405, 904–905.

Kim, Y., Kimball, J., Zhang, K., McDonald, K., 2012. Satellite detection of increasing Northern Hemisphere non-frozen seasons from 1979 to 2008: implications for regional vegetation growth. Remote Sens. Environ. 121, 472–487.

Kim, Y., Kimball, J.S., Glassy, J., McDonald, K.C., 2014. MEaSUREs Global Record of Daily Landscape Freeze/Thaw Status, Version 3. NASA National Snow and Ice Data Center Distributed Active Archive Center, Boulder, Colorado USA http://dx.doi.org/10.5067/MEASURES/CRYOSPHERE/nsidc-0477.003.

Kimball, J., McDonald, K., Keyser, A., Frolking, S., Running, S., 2001. Application of the NASA scatterometer (NSCAT) for classifying the daily frozen and non-frozen landscape of Alaska. Remote Sens. Environ. 75, 113–126.

Kimball, J., McDonald, K., Frolking, S., Running, S., 2004. Radar remote sensing of the spring thaw transition across a boreal landscape. Remote Sens. Environ. 89, 163–175.

McColl, K., Roy, A., Derksen, C., Konings, A., Alemohammed, S., Entekhabi, D., 2016. Triple collocation for binary and categorical variables: application to validating landscape freeze/thaw retrievals. Remote Sens. Environ.

McDonald, K., Kimball, J., Njoku, E., Zimmerman, R., Zhao, M., 2004. Variability in springtime thaw in the terrestrial high latitudes: monitoring a major control on the biospheric assimilation of atmospheric CO_2 with spaceborne microwave remote sensing. Earth Interact. 8, 020.

Mortin, J., Schrøder, T., Walløe Hansen, A., Holt, B., McDonald, K.C., 2012. Mapping of seasonal freeze-thaw transitions across the pan-Arctic land and sea ice domains with satellite radar. J. Geophys. Res. 117, C08004. http://dx.doi.org/10.1029/2012JC008001.

Panneer Selvam, B., Laudon, H., Guillemette, F., Berggren, M., 2016. Influence of soil frost on the character and degradability of dissolved organic carbon in boreal forest soils. J. Geophys. Res. Biogeosci. 121:829–840. http://dx.doi.org/10.1002/2015JG003228.

Piepmeier, J., Chan, S., Chaubell, J., Peng, J., Bindlish, R., Bringer, A., Colliander, A., De Amici, G., Dinnat, E., Hudson, D., Jackson, T., Johnson, J., Le Vine, D., Meissner, T., Misra, S., Mohammed, P., Entekhabi, D., Yueh, S., 2016. SMAP Radiometer Brightness Temperature Calibration for the L1B_TB, L1C_TB (Version 3), and L1C_TB_E (Version 1) Data Products, SMAP Project, JPL D-56295. Jet Propulsion Laboratory, Pasadena, CA https://nsidc.org/sites/nsidc.org/files/files/D56295%20SMAP%20L1C_TB_E%20Assessment%20Report.pdf.

Podest, E., McDonald, K., Kimball, J., 2014. Multisensor microwave sensitivity to freeze/thaw dynamics across a complex boreal landscape. IEEE Trans. Geosci. Remote Sens. 52 (11), 6818–6828.

Rautiainen, K., Lemmetyinen, J., Pulliainen, J., Vehviläinen, J., Drusch, M., Kontu, A., Kainulainen, J., Seppänen, J., 2012. L-Band radiometer observations of soil processes in boreal and subarctic environments. IEEE Trans. Geosci. Remote Sens. 50 (5), 1483–1497.

Rautiainen, K., Lemmetyinen, J., Schwank, M., Kontu, A., Ménard, C., Mätzler, C., Drusch, M., Wiesmann, A., Ikonen, J., Pulliainen, J., 2014. Detection of soil freezing from L-band passive microwave observations. Remote Sens. Environ. 147, 206–218.

Rautiainen, K., Parkkinen, T., Lemmetyinen, J., Schwank, M., Wiesmann, A., Ikonen, J., Derksen, C., Davydov, S., Davydova, A., Boike, J., Langer, M., Drusch, M., Pulliainen, J., 2016. SMOS prototype algorithm for detecting autumn soil freezing. Remote Sens. Environ.

Reichle, R., De Lannoy, G., Koster, R.D., Crow, W.T., Kimball, J.S., 2016. SMAP L4 9 km EASE-grid Surface and Root Zone Soil Moisture Geophysical Data, Version 2. NASA National Snow and Ice Data Center Distributed Active Archive Center, Boulder, Colorado USA http://dx.doi.org/10.5067/YK70EPDHNF0L.

Roy, A., Royer, A., Derksen, C., Brucker, L., Langlois, A., Mialon, A., Kerr, Y., 2015. Evaluation of spaceborne L-band radiometer measurements for terrestrial freeze/thaw retrievals in Canada. IEEE J. Sel. Top. Appl. Earth Obs. Remote Sens. http://dx.doi.org/10.1109/JSTARS.2015.2476358.

Schwank, M., Stähli, M., Wydler, H., Leuenberger, J., Mätzler, C., Flühler, H., 2004. Microwave L-band emission of freezing soil. IEEE Trans. Geosci. Remote Sens. 42 (6), 1252–1261.

Vaganov, E.A., Hughes, M., Kirdyanov, A., Schweingruber, F., Silkin, P., 1999. Influence of snowfall and melt timing on tree growth in subarctic Eurasia. Nature 400, 149–151.

Wang, L., Derksen, C., Brown, R., 2013. Recent changes in pan-Arctic melt onset from satellite passive microwave measurements. Geophys. Res. Lett. 40. http://dx.doi.org/10.1002/grl.50098.

Wang, T., Peng, S., Krinner, G., Ryder, J., Li, Y., Dantec-Nédélec, S., et al., 2015. Impacts of satellite-based snow albedo assimilation on offline and coupled land surface model simulations. PLoS One 10 (9), e0137275. http://dx.doi.org/10.1371/journal. pone.0137275.

Watanabe, M., Kadosaki, G., Kim, Y., Ishikawa, M., Kushida, K., Sawada, Y., Tadono, T., Fukuda, M., Sato, M., 2011. Analysis of the sources of variation in L-band backscatter from terrains with permafrost. IEEE Trans. Geosci. Remote Sens. 50 (1), 44–54.

West, et al., 2016. SMAP L1C Radar Half-orbit 3 km EASE-grid Backscatter, Version 3, SMAP_L1C_S0_HiRes_V3, Fairbanks, Alaska USA. Alaska Satellite Facility http://dx.doi.org/10.5067/NVVUJ0MNG3PN.

Xu, X., Derksen, C., Yueh, S., Dunbar, R.S., Colliander, A., 2016. Freeze/thaw detection and validation using Aquarius L-band backscattering data. IEEE J. Sel. Top. Appl. Earth Obs. Remote Sens. 9 (4):1370–1381. http://dx.doi.org/10.1109/JSTARS.2016.2519347.

Zhang, K., Kimball, J., Kim, Y., McDonald, K., 2011. Changing freeze-thaw seasons in northern high latitudes and associated influences on evapotranspiration. Hydrol. Process. 25:4142–4151. http://dx.doi.org/10.1002/hyp.8350.